Store Release Trajectory Variability from Weapon Bays using Scale Adaptive Simulations

G.J.M. Loupy[1] , G.N. Barakos[2]

CFD Laboratory, University of Glasgow, Glasgow, G12 8QQ, UK

N.J. Taylor[3]

MBDA UK Ltd, Filton, Bristol, BS34 7QW, UK

Abstract

In this paper, scale-adaptive simulation is used to study store trajectory variability for releases from transonic weapon bays. The scale-adaptive simulation captures the essential physics of the flow in the weapon bay, and its speed of computation allows for several trajectories to be computed within reasonable time. The results of the simulations are treated as a statistical set and a metric is put forward to decide the minimum number of simulations necessary to establish the mean and the standard deviation of the releases. Averaging the results of all trajectories was useful in developing an overall understanding of the bay pressure field role on the store trajectories. Filtering the obtained trajectories provided insight in the flow frequencies affecting the forces acting on the store and the coordinates of its CG during releases. For the store employed in this study, less than 1 month of CPU time is needed for the complete set of simulations to be obtained making this method promising as a further test before flight testing.

[1]PhD Student. g.loupy.1@research.gla.ac.uk

[2]Professor, MAIAA, MRAeS, MAHS. george.barakos@glasgow.ac.uk, cor. author

[3]Capability Leader, MBDA UK Ltd., AIAA Assoc. Fellow, nigel.j.taylor@mbda.co.uk

Latin

C_p	Pressure coefficient (-)
C_x, C_y, C_z	Axial, side and normal force coefficients (-)
C_l, C_m, C_n	Rolling, pitching and yawing moment coefficients (-)
D	Cavity depth (m)
d_{ref}	Store reference diameter (m)
f	Frequency (Hz)
$I_x,\ I_y,\ I_z$	Moment of inertia of the store $(kg.m^2)$
k	Specific turbulent kinetic energy (m^2/s^2)
L	Cavity length (m)
L_s	Store length (m)
m_s	Mass of the store (kg)
M_∞	Free-stream Mach number (-)
p, q, r	roll, pitch and yaw rates (deg/s)
p	Pressure (Pa)
q_s	Free-stream dynamic pressure (Pa)
Q	Adimensional flow momentum (-)
Re_L	Reynolds number based on cavity length (-)
S	Base area of the store (m^2)
u, v, w	Velocity components (m/s)
t	Time (s)
U_∞	Free-stream Velocity (m/s)
W	Cavity width (m)
W_e	Maximum envelope width
X, Y, Z	Cartesian coordinates (m)
X_b, Y_b, Z_b	Store reference coordinates (m)

Greek

Δ	Statistical convergence index
$\mu(t, n)$	Average of n trajectories(-)
ω	Specific turbulence dissipation rate (1/s)
ϕ, θ, ψ	Roll, pitch and yaw angles (deg)
ρ	Density (kg/m^3)

Acronyms

AEDC	Arnold Engineering Development Center
CFD	Computational Fluid Dynamics
CG	Gravity Center
DES	Detached Eddy Simulation
FS	Full Stroke
HS	Half Stroke
HMB	Helicopter Multi-Block
LES	Large Eddy Simulation
MFRT	Minimum Frequency to Reconstruct Trajectory
NED	North East Down
RK4	Runge-Kutta method 4th order
SAS	Scale Adaptive Simulation
SST	Shear Stress Transport
6DoF	Six-Degree of Freedom

1 Introduction

Weapon bays enhance the stealth of modern military aircraft. However, when exposed to the air flow during store delivery, those cavities generate strong acoustic fields. Their noise comprises broadband and tonal noise, called Rossiter modes [1], produced by a complex interaction between the shear layer and the aft bay wall [2, 3].

The acoustic field around an ideal cavity is well studied as documented in Lawson and Barakos [4]. For weapon bays, their unsteady flow affects the loads on the released stores, and leads to trajectory variability. To guarantee safe store separation from weapon bays, the statistics of the trajectories have to be known. Although effective, flight tests [5] are expensive, and limited at critical conditions[6]. On the other hand, weapon bay flows can be simulated with CFD using Detached Eddy Simulation (DES), or Large Eddy Simulation (LES) [7]. As shown by Babu *et al.*[8] Scale-Adaptive Simulations (SAS) [9] can reduce the simulation time almost by an order of magnitude, and resolve well the cavity flow. This means that practical calculations of store releases, and statistical analyses of their trajectory variability are now possible.

CFD studies of store releases are rare, and few use a time accurate approach [10, 11, 12, 13], coupling CFD with a 6DoF method to compute the models trajectory. Kim *et al.*[14] computed releases using $k - \omega$ SST and DES from an ideal cavity at Mach 0.95. Four drops at different time instances showed trajectory variability due to changes in the store loads. The same drops repeated with steady blowing at the leading lip of the cavity appeared to reduce the variability. Nevertheless, studying store release variability is challenging, and more work is needed to explain the relationship between the fluctuations in the store loads and the obtained trajectories.

In view of the above, this paper presents the first statistical study on trajectory variability using coupled computations employing high fidelity CFD and Six Degree of Freedom model of the store. This work treats the store release problem in a statistical way analysing several trajectories. The paper suggests a statistical metric to decide the number of trajectories needed to quantify variability. In addition, analysis of the results using filtering, reveals the origin of trajectory variability and its relationship with the inertial properties of the store.

2 CFD Methodology

2.1 CFD Solver

The Helicopter Multi-Block (HMB3) [15] code is used in the present work. The solver is described in references [8, 16, 17, 18] and has been extensively validated for cavity flows. DES is by far the most common way to account of the effect of the turbulence of cavity flows. Nevertheless, DES is still expensive especially when several computations of store releases are necessary. In order to investigate trajectory variability, promising results with SAS method [9] encouraged Babu *et al.*[8] to use this approach for weapon bay flows. Their results suggest that SAS captures the essential physics of the weapon bay, and at the same time, provides a significant reduction of CPU time by almost an order of magnitude. For this reason SAS is also used in the present work. Only the 6DoF method used for store trajectory is shown here.

2.2 6DoF Method

The store motion during release was described using six rigid-body degrees of freedom (three body position coordinates and three body attitudes) and was strongly coupled with HMB3. This approach assumes that store release computations use the chimera method, so that a store has its own grid. The store motion is described using earth and store reference systems. The earth system uses the North East Down (NED) convention where, X is positive north, Y is positive east and perpendicular to X axis, and Z is positive towards the earth centre. The store system X_b, Y_b, Z_b is right-handed and coincident with the earth system at carriage, with respect to the roll, pitch and yaw axes. The store translation is described using the earth system, and the store rotations using Euler angles and the store system. The computed position and orientation are applied at every instance in time to the store grid. Force and moment coefficients acting on the store, as obtained from
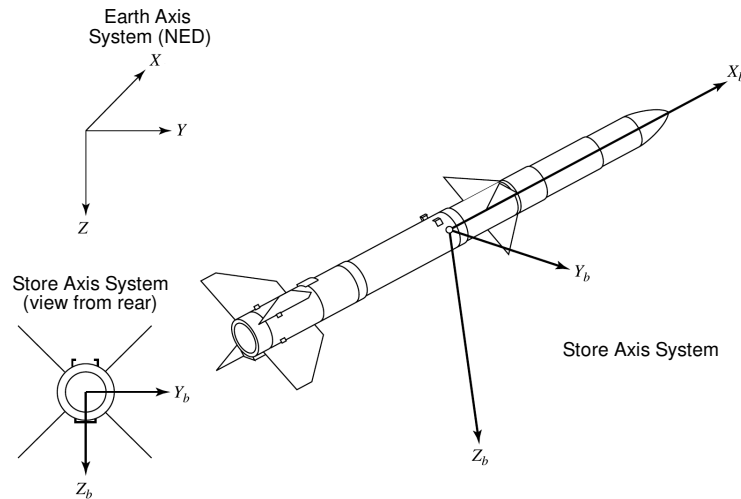
Figure 1: Orientation of store axes with respect to the earth axes [19].

HMB3, are applied into the translational and rotational equations of motion [19] of a store in body axes:

Longitudinal Acceleration: $\dfrac{du}{dt} = rv - qw - g\sin\theta(C_x q_s S)/m_s,$ (1)

Lateral Acceleration: $\dfrac{dv}{dt} = pw - ru + g\cos\theta\sin\phi(C_y q_s S)/m_s,$ (2)

Vertical Acceleration: $\dfrac{dw}{dt} = qu - pv + g\cos\theta\cos\phi(C_z q_s S)/m_s,$ (3)

Roll Acceleration: $\dfrac{dp}{dt} = C_l(q_s S d_{ref}/I_x) + qr[(I_y I_z)/I_x],$ (4)

Pitch Acceleration: $\dfrac{dq}{dt} = C_m(q_s S d/I_y) + pr[(I_z I_x)/I_y],$ (5)

Yaw Acceleration: $\dfrac{dr}{dt} = C_n(q_s S d/I_z) + pq[(I_x I_y)/I_z].$ (6)

In the above, m_s is the mass of the store and q_s is the free-stream dynamic pressure. u, v and w are the velocity components of the store. p, q and r are the roll, pitch and yaw rates, respectively, of the store. C_x, C_y and C_z are the axial, side and normal force coefficients, respectively, and C_l, C_m and C_n are the rolling, pitching and yawing moment coefficients, respectively, acting on the store. C_m is positive nose up. d_{ref} is the store reference diameter and S its base area. I_x, I_y, I_z are the moments of inertia of the store about the X, Y and Z axis respectively. As the store used in this project is symmetric about the $X_b - Y_b$ plane, the off-diagonal products of inertia terms, are ignored.

The equations for the angular velocities[19] in terms of the Euler angles are then:

$$\frac{d\psi}{dt} = (q\sin\phi + r\cos\phi)/\cos\theta,$$ (7)

$$\frac{d\theta}{dt} = q\cos\phi - r\sin\phi,$$ (8)

$$\frac{d\phi}{dt} = p + (\frac{d\psi}{dt}).\sin\theta$$ (9)

The translational components are calculated in the earth axis system and the angular components are calculated using the Euler angles. The integration of the equations of motion are done with the Runge-Kutta method of order 4 (RK4). Figure 1 presents the employed frame of reference and the adopted conventions.

2.3 Solution Monitoring

In this work, the time is expressed in terms of cavity travel time, which is the time it takes for a flow particle moving at U_∞ to run the cavity length L.

The aerodynamic moments on the complete store (body and fins included) were computed about the store centre of mass. The force (C_{force}) and moment coefficients (C_{moment}) are computed using:

$$C_{force} = \frac{F}{\frac{1}{2}\rho_\infty U_\infty^2 S} \quad \text{and} \quad C_{moment} = \frac{M}{\frac{1}{2}\rho_\infty U_\infty^2 d_{ref} S} \tag{10}$$

where F and M are forces and moments, d_{ref} is the store diameter, and $S = \pi d_{ref}^2/4$ is the store reference area.

The boundaries of the shear layer are defined as the strictly positive values of Q, product between the flow momentum, and the local contribution to the displacement thickness of the shear layer. Negative values due to the cavity flow re-circulation are set to zero:

$$Q = max\left(0, \frac{\rho u}{\rho_\infty U_\infty}\left(1 - \frac{u}{U_\infty}\right)\right) \tag{11}$$

3 Validation of the CFD Method

The CFD method has been validated for the M219 cavity flow[20], and results can be found in reference [17]. Nevertheless, validation for store release separation is given here.

The following section presents validation of the 6DoF method in HMB3 for the widely used wind tunnel test conducted at the AEDC[21]. Several studies have utilised this test case, using structured[22, 23, 24, 25], unstructured[26, 27, 28, 29, 30, 31] and meshless solvers[32], to validate the prediction of the store trajectory, making it a popular validation case. The test provided pressure data for a geometrically simple wing and store under mutual interference as well as a realistic trajectory. AEDCs 4-Foot Transonic Aerodynamic Wind Tunnel (4T) was used for the test together with its captive trajectory support system to simulate the motion of the store and the Mach number was 0.95.

3.1   Model Geometry and Release Conditions

The computational model was based on the wind tunnel geometry as reported in [21] (Figure 2). The properties of the store and ejectors are summarised in table 1. While the wind tunnel test consisted of a wing, pylon and store configuration, the pylon was omitted from the computational model to simplify the overset mesh in the region where the pylon and the store are almost in contact. Nevertheless, good agreement was found in the loads between experiments and CFD. The wind tunnel test model was of 5% scale of a generic full-scale wing/pylon/store.
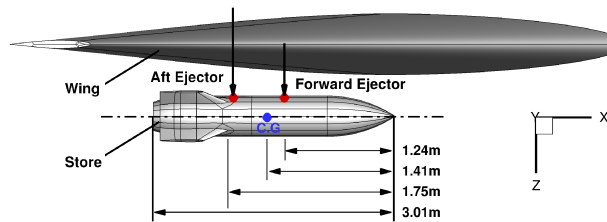

Figure 2: Wing store configuration and ejector position.

8

Characteristics	
Weight	8896.4 N
Centre of Gravity	1.41 m (aft of store nose)
Roll Inertia (I_x)	27.12 $kg.m^2$
Pitch Inertia (I_y)	488.1 $kg.m^2$
Yaw Inertia (I_z)	488.1 $kg.m^2$
Forward Ejector Location	1.24 m (aft of store nose)
Forward Ejector Force	10675.7 N
Aft Ejector Location	1.75 m (aft of store nose)
Aft Ejector Force	42702.9 N
Ejector Stroke Length	0.1 m

Table 1: Full-scale store and ejector characteristics[21].

3.2 Decoupled Analysis

Prior to running a fully coupled trajectory computation in HMB3, a decoupled approach was taken to compare the wind tunnel trajectory to that obtained from the 6DoF method in HMB3. Force and moment coefficients from the wind tunnel data were used as input. In this way the 6DoF method is tested without the expense of computing the flow at every instance in time.

Figure 3 shows a comparison of the wind tunnel trajectory to the trajectory computed by the 6DoF method in HMB3 through the decoupled approach, for the full available signal length of 0.92s. WT is the wind tunnel data, and NUM the decoupled results from HMB3. Velocity components and CG displacements agreed well with wind tunnel data, however small differences can be seen in the pitch and yaw rates and hence the pitch and

9

(a) Velocities (m/s)

(b) CG Displacements (m)

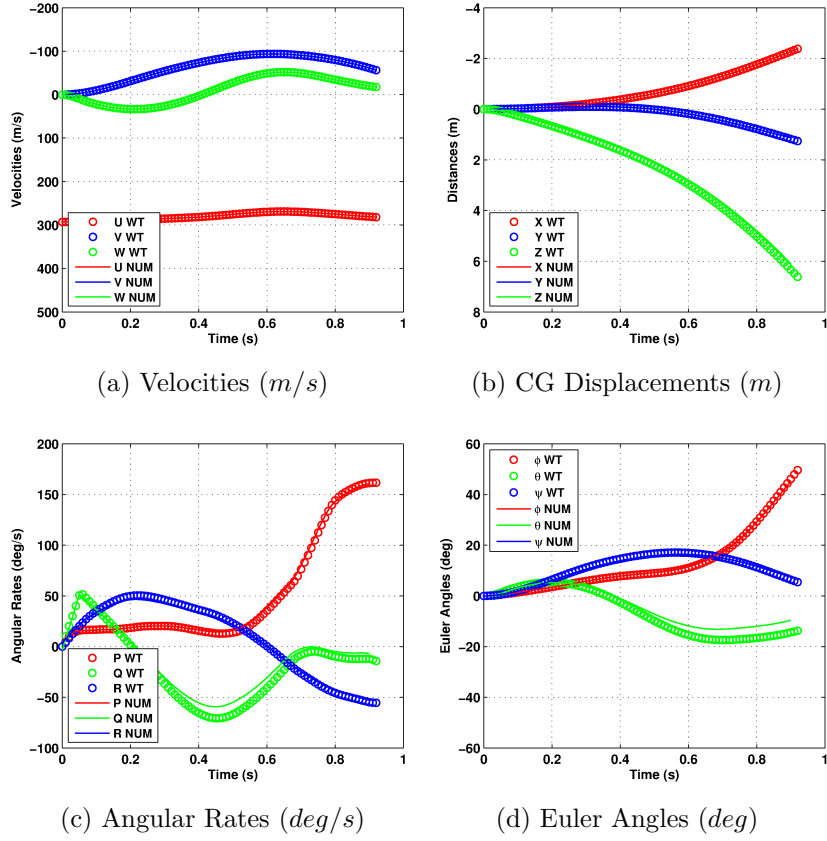(c) Angular Rates (deg/s)

(d) Euler Angles (deg)

Figure 3: Comparison of trajectories from a decoupled approach and wind tunnel data[21].

yaw angle. The initial part of the trajectory, controlled by the ejector forces compared closely to wind tunnel data, however, after about 0.3s the pitch and yaw rate started to drift away from wind tunnel data. This behaviour over time, especially in pitch rate and attitude, was also reported in previous studies[22, 28, 29].

3.3 Store Loads and Trajectory

Computations were run at a Mach number of 0.95 and Reynolds number of $1.0.10^6$ (based on the root chord of the wing). The store release computation, solving the Euler equations of motion, was initiated from a solution around the store at carriage position, after the flow was fully developed. The store loads obtained through HMB3 agreed with the wind tunnel data. Figure 4 shows the trajectory of the store starting from the carriage position at time $t = 0.0s$ with a time step of 0.1s computed with HMB. The trajectory visualised here shows the store having an initial nose-up pitching moment as expected from the difference in force between the forward and aft ejectors. The store recovers from the pitch, and is seen to have a growing positive yawing moment over time.
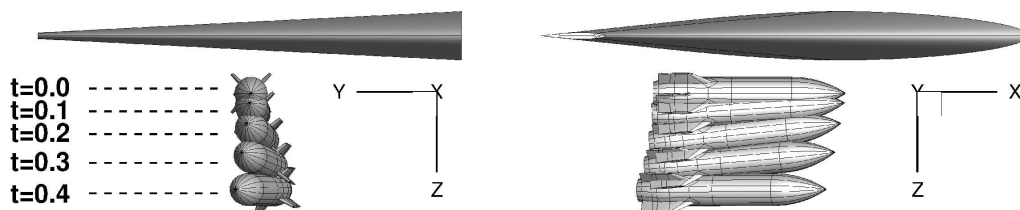

Figure 4: Store trajectory released from the wing at different time instances.

Figure 5 presents a comparison of the trajectory computed using HMB3 and the wind tunnel data. The forces, velocities, displacements, moments, angular rate and Euler angles, in the missile axes, were compared for 0.4s of the simulation. It is apparent that the force coefficients, velocity and location of the CG closely matched the wind tunnel data. The store moved slightly rearward and inboard as it moved further away from the wing. Small discrepancies were seen in the moment coefficients that were carried into the angular rates and Euler angles.
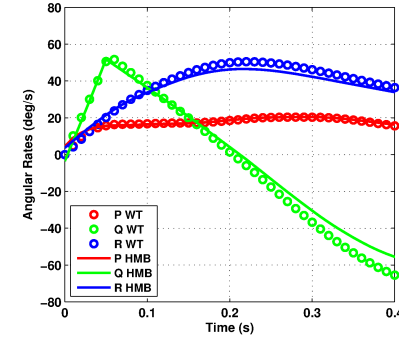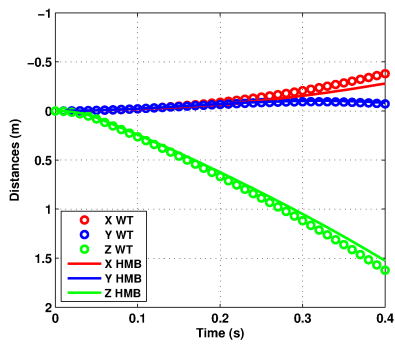
11
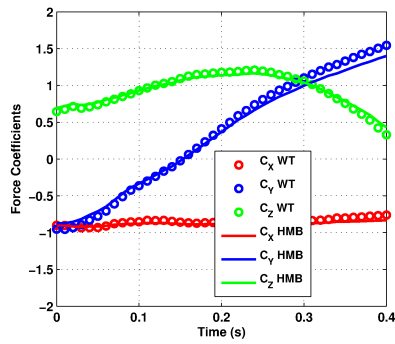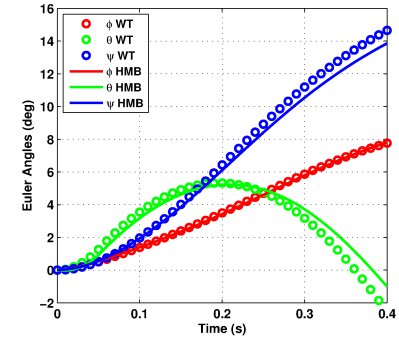
(a) Force Coefficients
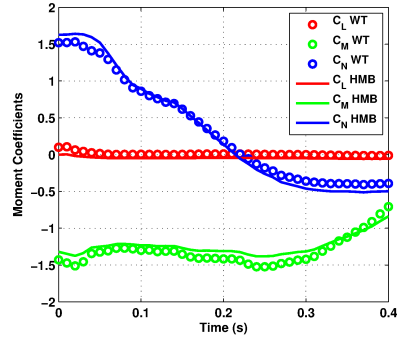
(b) Moment Coefficients
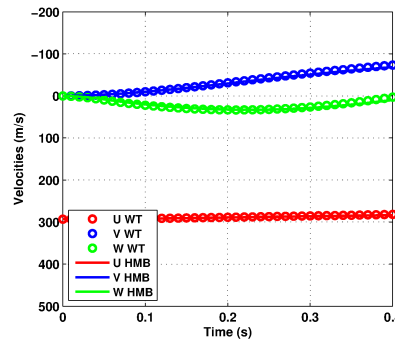
(c) Velocities (m/s)

(d) Angular Rates (deg/s)

(e) CG Displacements (m)

(f) Euler Angles (deg)

Figure 5: Trajectories comparison between HMB3 and wind tunnel data[21].
WT: Wind tunnel.

Initially, there was a slight underprediction of the rolling moment and overprediction of the pitching and yawing moment coefficients. The initial overprediction in the pitching moment coefficient did not affect the initial part of the trajectory in terms of gravity center location or pitch attitude as the ejector and gravity forces dominated the aerodynamic forces and moments in that direction.

The effect of the ejectors is seen clearly in the pitch rate that grows positively for the initial 0.5 seconds of the release. Once the ejector stroke ended, the aerodynamic pitching moment on the store began to reduce. The pitch and yaw curves showed a slight divergence from the wind tunnel data after about 0.3 seconds of the release. This divergence over time was not only observed in the original study by Fox[21], but in other studies[22, 28, 29] as well.

4 Geometric and Computational Model for Trajectory Variability

The computations were carried using HMB3 and the Scale-Adaptive Simulation with a timestep equal to 1% of the cavity length travel time (0.12ms). The cavity mesh was composed of 30.5 million cells, and the store mesh of 4.2 million cells. The free-stream Mach number was 0.85 and the Reynolds number based on the cavity length (Re_L) was 6.5 million (Figure 6). The cavity had a length to depth ratio of 7, and was 3.59m long, and 1.03m wide. The store is 90% of the cavity length with four fins in a cross configuration. The non dimensional moments of inertia $I/(m_s.L_s^2)$ are $4, 0.10^{-4}$ about the roll axis and $7, 3.10^{-2}$ about the pitch and yaw axes, with the centre gravity

13

at mid length.
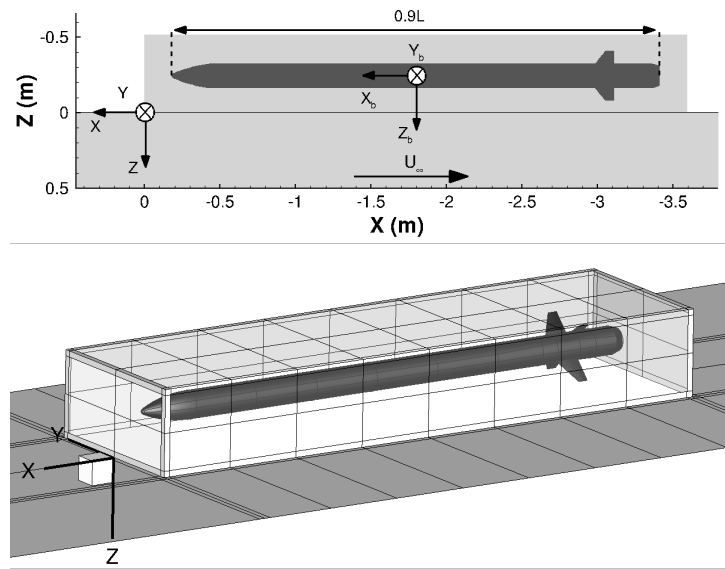

Figure 6: Geometry, cavity axes, and the store at carriage position.

The store release included three phases. At *carriage* (Z/D=-0.5), the store was fixed while the flow was allowed to develop. Then, during the *stroke phase*, the store was pushed towards the cavity opening. During this phase, a vertical velocity of 5m/s was imposed on the store, with other degrees of freedom set to zero. This phase ended when the stroke length was reached. The full stroke was half a cavity depth (0.257m). In addition, a half stroke was also used (0.129m). Finally the store was free to move under the aerodynamic forces. Twenty computations were carried out, 5 applying a full stroke (FS) length and 15 applying a half stroke (HS) length, at different release times. The computations are summarised table 2.

14

ID	Stroke Start Travel Time / Time (ms)	Stroke Length (m)
FS2000	20 / 13	0.257
FS2400	24 / 62	0.257
FS2600	26 / 87	0.257
FS3000	30 / 137	0.257
FS3400	34 / 187	0.257
HS2000	20 / 13	0.129
HS2200	22 / 37	0.129
HS2400	24 / 63	0.129
HS2600	26 / 87	0.129
HS2800	28 / 113	0.129
HS3000	30 / 137	0.129
HS3200	32 / 162	0.129
HS3400	34 / 189	0.129
HS3600	36 / 212	0.129
HS3800	38 / 238	0.129
HS4000	40 / 263	0.129
HS4200	42 / 289	0.129
HS4600	46 / 339	0.129
HS5000	50 / 390	0.129
HS5400	54 / 440	0.129

Table 2: List of computations carried out to demonstrate the trajectory variability.

5 Results and Discussion

5.1 Statistical Analysis of the Trajectories

Figures 7a and 7b present the vertical velocity w, and the displacement Z for the full and half stroke releases, as functions of time. The variability is negligible, of the order of 5cm, and the vertical displacement Z appears to be mainly driven by gravity. For a better reading, the trajectories are shown as function of Z/D in the following. The longitudinal and the span-wise amplitudes of displacement, not shown in the figures, are of the order of 1 cm, and are also negligible compared to the vertical displacement. The store angles shown in figure 7 have broader variability, with the roll angle varying between -5 and 6 degrees, the pitch between 2 and 4 degrees, and the yaw between -1 and 1 degrees at one cavity depth away from the cavity opening (Z/D=1). The roll rate reaches peak values (up to 80deg/s), and the curves have more frequency content compared to the pitch and yaw angles.

Amongst other possible criteria, statistical convergence is tested here using the maximum of the normalised difference between the average of n+1, and n trajectories:

$$\Delta_\mu = \frac{max|\mu(t, n + 1) - \mu(t, n)|}{W_e} \tag{12}$$

with $\mu(t, n)$ the average of n trajectories, where t covers the complete time of simulation. The envelope of the trajectory is defined as the maximum difference between minimum, and maximum over all the releases and all store vertical positions. W_e is the largest envelope width over all positions, and indicated by dashed lines in figures 7 and 10. Figure 8 shows the convergence of the proposed metric for all store releases in a random order. A trajectory component is considered as converged if the difference (Δ_μ) between two con-
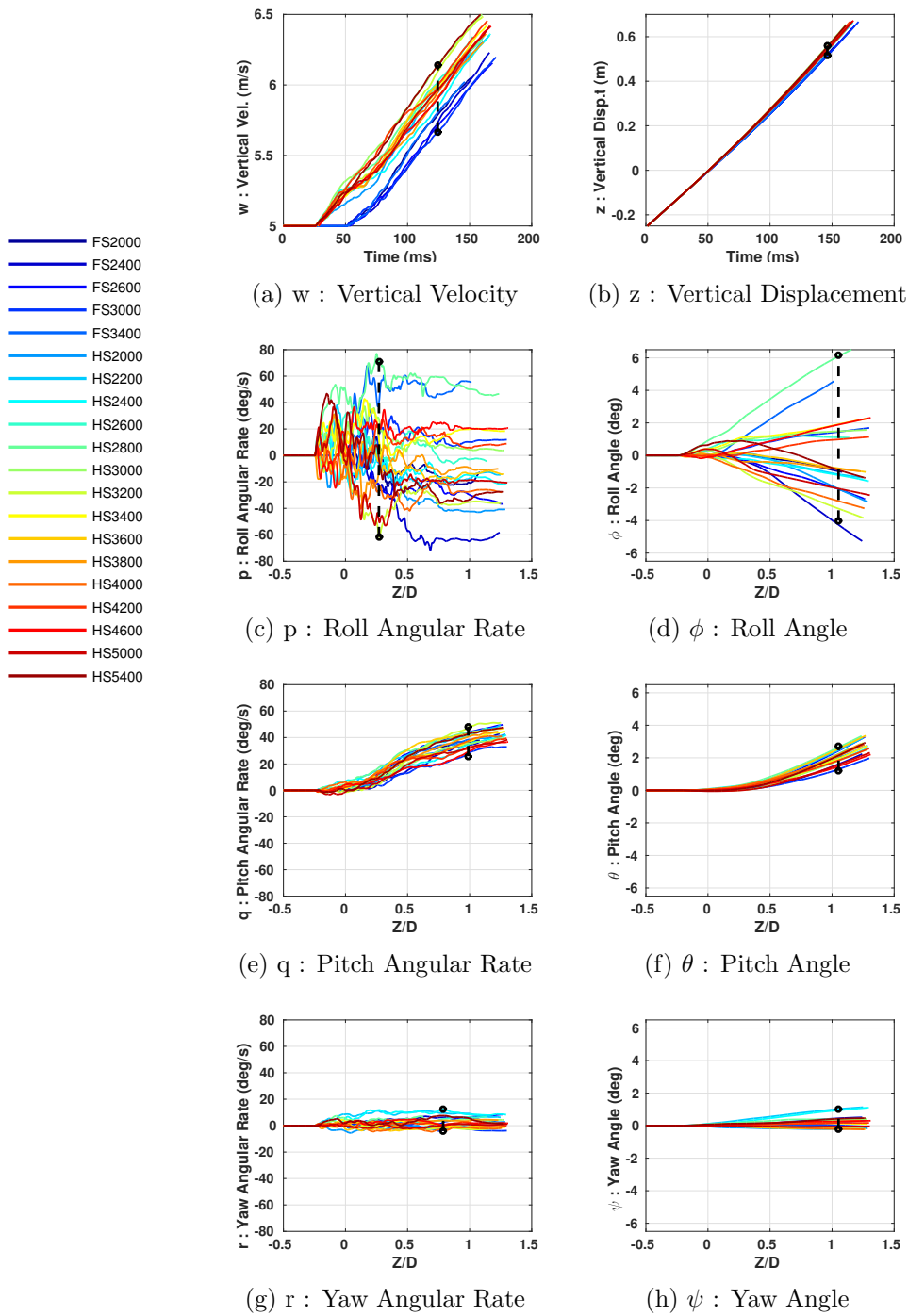
16

Legend:
FS2000, FS2400, FS2600, FS3000, FS3400, HS2000, HS2200, HS2400, HS2600, HS2800, HS3000, HS3200, HS3400, HS3600, HS3800, HS4000, HS4200, HS4600, HS5000, HS5400

(a) w : Vertical Velocity

(b) z : Vertical Displacement

(c) p : Roll Angular Rate

(d) ϕ : Roll Angle

(e) q : Pitch Angular Rate

(f) θ : Pitch Angle

(g) r : Yaw Angular Rate

(h) ψ : Yaw Angle

Figure 7: Trajectory of full and half stroke cases.

17

secutive averages is less than 5%. As can be seen in figure 15, the averages substantially fluctuate with less than 10 drops due to the flow variability. For example, the roll angle may even change sign for two consecutive releases. The number of releases to converge the statistics depends on the order of the
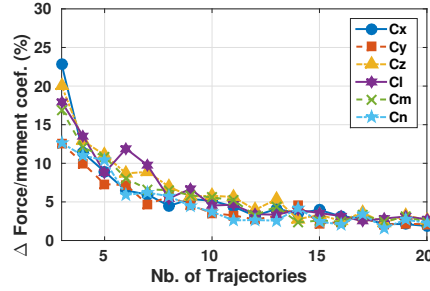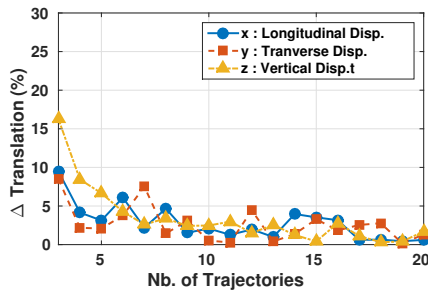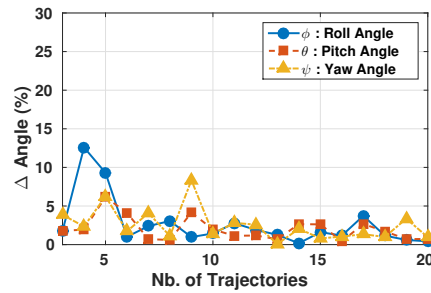

(a) Forces and Moments
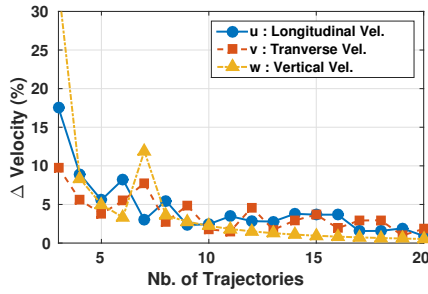
(b) Velocity
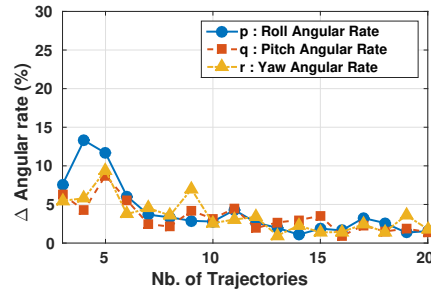
(c) Angle Rate

(d) Translation

(e) Angle

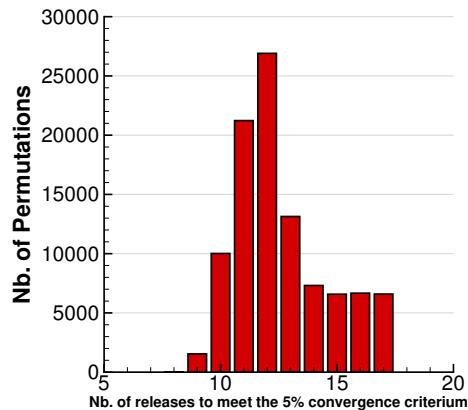Figure 8: Convergence of the averaged trajectory.

18

Figure 9: Number of release required to reach convergence.

trajectories. To minimise this effect, Δ_μ is computed for 100.000 random trajectory permutations. For each permutation, the number of releases required to converge the statistics is computed, and figure 9 summarises the number of permutations. On average, the statistics converge with 12.6 releases, and after 17 releases, the average is always converged. Consequently, this average is seen as converged for this case, and the results can now be used to compute a mean flow and assess its effects on the trajectory.

Figure 10 shows the forces driving the trajectories. The curves appear to be very noisy. The largest variability is seen for the roll angle that is sensitive to the high flow frequencies, due to the roll inertia being two orders of magnitude smaller than the inertia in pitch and yaw.

5.2   Mean Flow

Taking all the trajectories with full and half stroke, an averaged trajectory was constructed, considering all times of the simulations from stroke initiation until a common point in time corresponding to the shortest of the
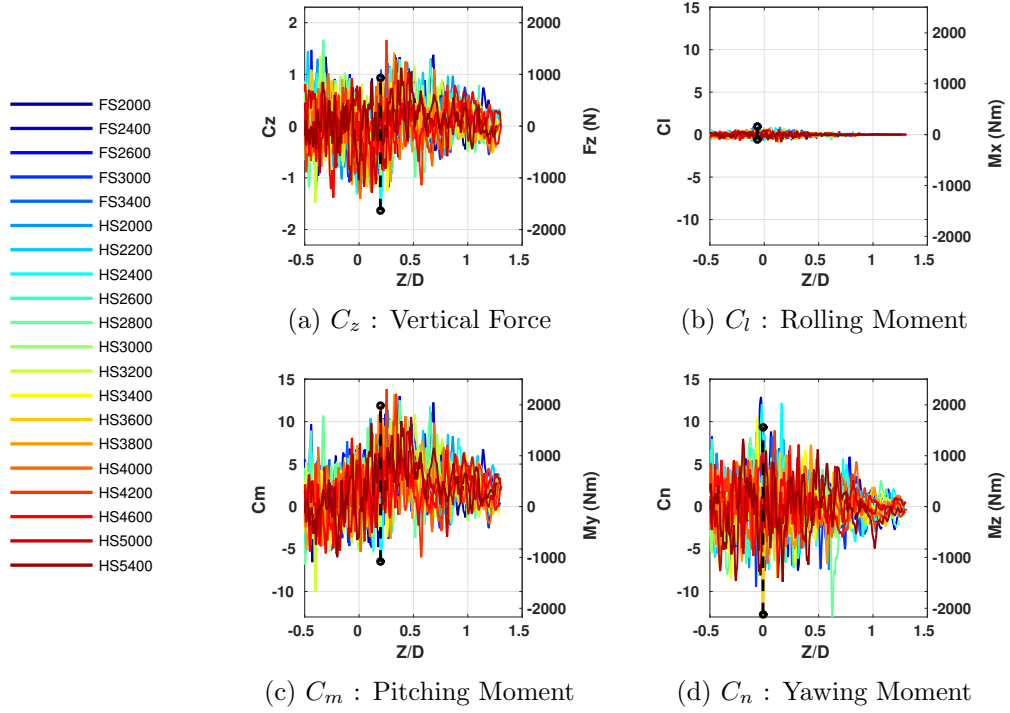
Figure 10: Force and moment coefficients during full and half stroke releases.

simulated trajectories (FS3400). Figure 11 shows the average trajectory in continuous lines, and the standard deviation in dashed lines, for the vertical store displacement, and all store rotations. The vertical velocity does not increase linearly during the release, as a strong normal aerodynamic force appears when the store interacts with the shear layer at Z/D=0.2. The averaged pitch angle grows with the distance from the cavity, and the pitching moment reaches a peak at Z/D=0.35.

Figures 12a and 12b show the distributions of vertical force C_z and pitching moment C_m coefficients along the store length, averaged over all releases. The loads were integrated on the store body and fins, in sections of 3.5% of the store length, and the vertical axis represents the store CG position
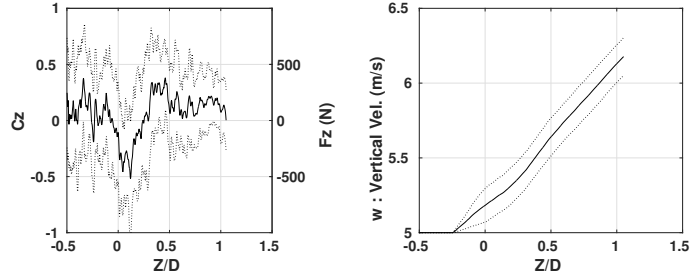
(a) C_z : Vertical Force

(b) w : Vertical Velocity
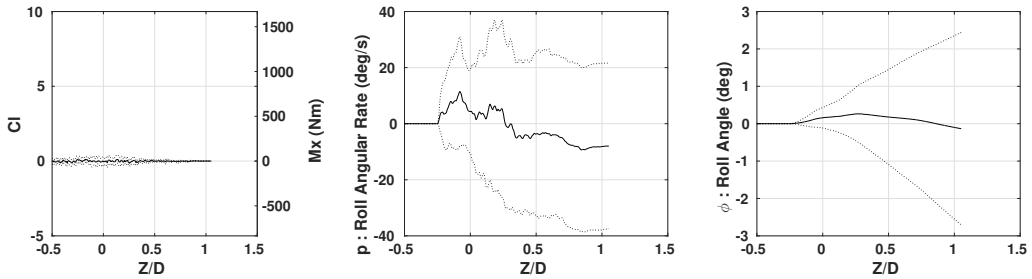
(c) C_l : Rolling Moment

(d) p : Roll Angular Rate

(e) ϕ : Roll Angle
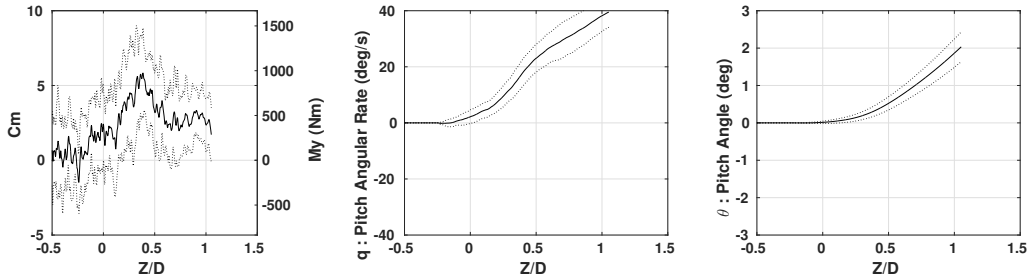
(f) C_m : Pitching Moment

(g) q : Pitch Angular Rate

(h) θ : Pitch Angle
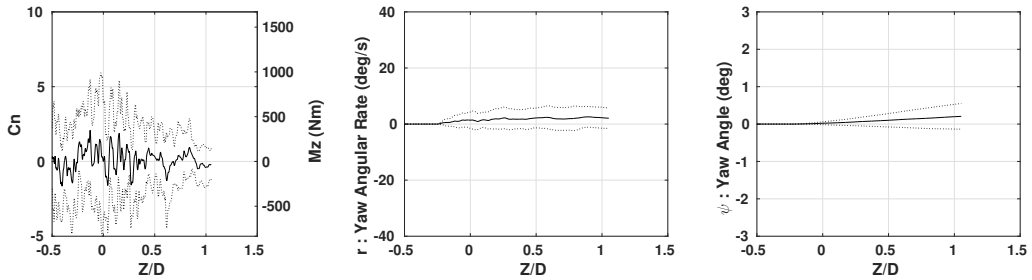
(i) C_n : Yawing Moment

(j) r : Yaw Angular Rate

(k) ψ : Yaw Angle

Figure 11: Averaged translations and rotations with half and full stoke releases.

21

during the release. The two main sources of loads are localised near the front of the store, where the flow encounters the store nose, and near the fins. The C_p distribution averaged over all releases is also shown at the mid-span plane of the cavity (Figures 12c to 12f). The averaged results are shown

(a) C_z : Vertical Force

(b) C_m : Pitching Moment

(c) C_p $-0.40 < Z/D < -0.30$ (Inside)

(d) C_p $0.00 < Z/D < 0.10$ (Shear Layer)

(e) C_p $0.35 < Z/D < 0.45$ (Max C_m)

(f) C_p $0.90 < Z/D < 1.00$ (Away)

Figure 12: Averaged store loads, and pressure coefficient at cavity mid-span.

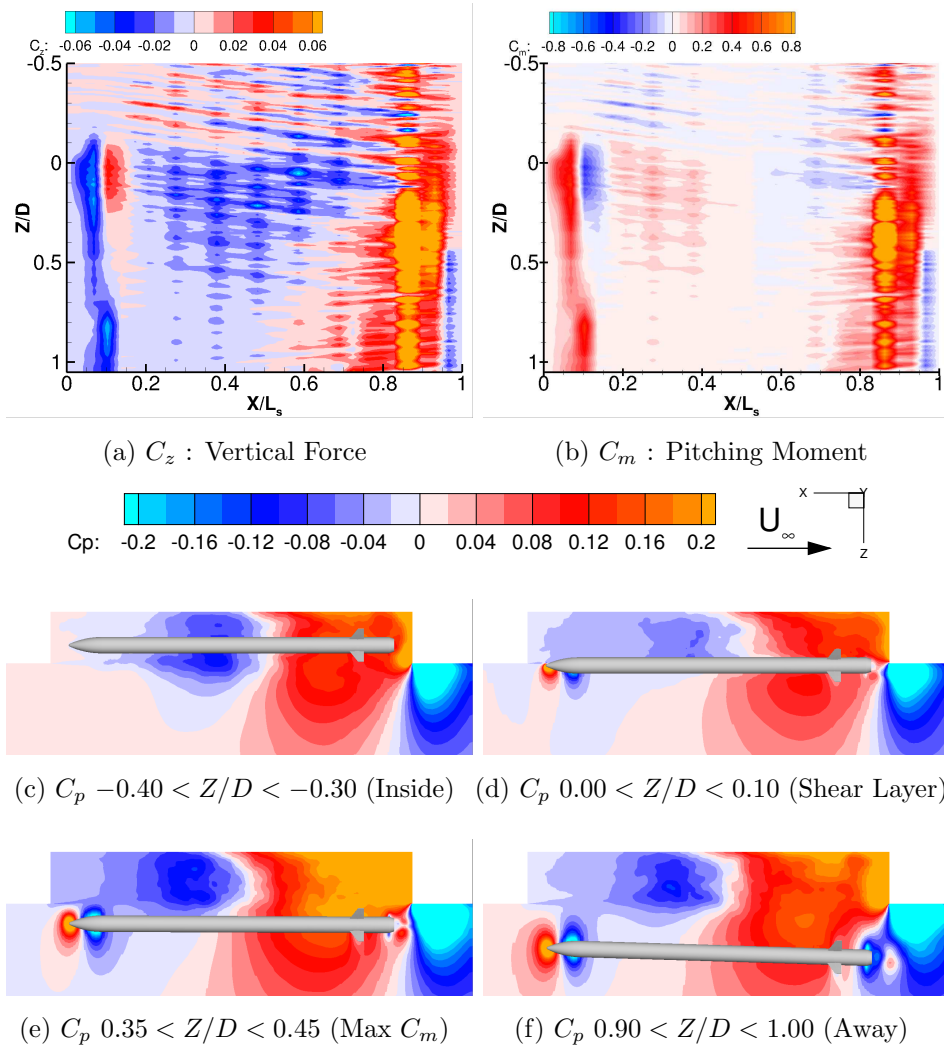for four bands: for the store inside the cavity ($-0.40 < Z/D < -0.30$), at the shear layer ($0.00 < Z/D < 0.10$), at the peak of pitching moment C_m ($0.35 < Z/D < 0.45$) and far from the cavity ($0.90 < Z/D < 1.00$).

Inside the cavity (Figure 12c), a small pressure gradient between the upper and bottom surfaces of the store, explains the small averaged loads at this position, and the small differences between full and half stroke releases. When the store crosses the bay opening (Figure 12d), it is at the interface between the cavity and the free-stream conditions, leading to a strong average pressure gradient at its mid length. A further contribution to the aerodynamic normal force is due to the impact of the shear layer on the store nose. Nevertheless, the effects of the ejector push and gravity dominate. Away from the cavity, at the peak of pitching moment (Figure 12e), there is a large increase of the pressure at the aft cavity wall, leading to an increase of the vertical force on the fins, and to the peak of pitching moment. The free-stream impacting on the pitched store nose, also contributes to the larger pitching moment at this position. Going further away (Figure 12f), the pressure gradients due to the cavity flow decrease, and the loads at the store nose and the fins dominate.

Using equation 11, the flow momentum is shown in figure 13 averaged over all releases at the previous store positions, inside the cavity, at shear layer, at the peak of pitching moment, and far from the cavity. As the store travels towards the far-field, the shear layer is deflected into the cavity by the store, more than for the clean cavity flow. This results in a pressure peak at the aft wall, leading to the peak of pitching moment. Away from the cavity, the store effect reduces, and the shear layer becomes characteristic of a clean cavity flow.
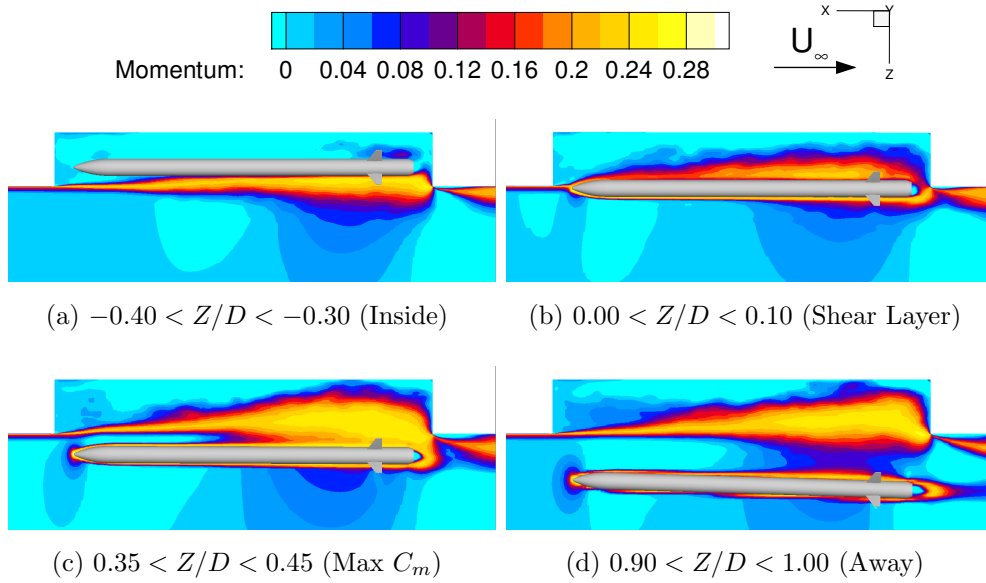
23

(a) $-0.40 < Z/D < -0.30$ (Inside)   (b) $0.00 < Z/D < 0.10$ (Shear Layer)

(c) $0.35 < Z/D < 0.45$ (Max C_m)   (d) $0.90 < Z/D < 1.00$ (Away)

Figure 13: Flow momentum at the cavity mid-span.

5.3 Filtered Loads

The store forces are decomposed in pressure and viscous contributions for release HS2600 (Figure 14). All trajectory components are driven by the pressure forces, and only the drag force (C_x) noticeably depends on viscosity. Store angles not shown here are also driven by pressure forces. The load fluctuations driving the trajectory variability are very noisy, and difficult to interpret (Figure 15). To determine the frequency bands that drive the trajectories, a low pass Butterworth filter of 4th order is applied to the signals, minimising the band overlapping, and signal distortion [33]. The Butterworth filter have some advantages in processing noisy signals removing the highest frequencies without affecting the main tones. In the following, trajectories computed with unfiltered loads are denoted as "original", in contrast to the "filtered" ones. For each trajectory, the Minimum Frequency required

(a) Pressure forces   (b) Viscous forces
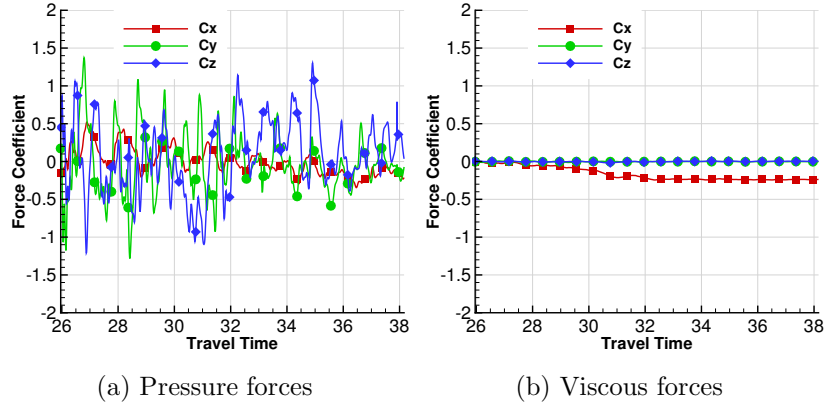
Figure 14: Decomposition of the HS2600 store forces in pressure and viscous components.

(a) Pitch Moment   (b) Pitch Angle
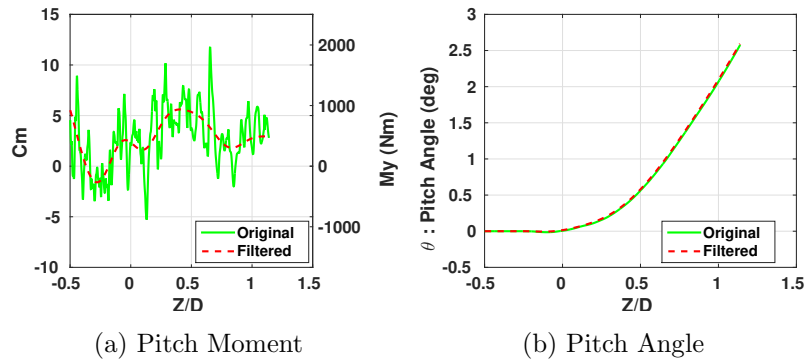
Figure 15: Original and filtered pitch for the case HS2600.

to Reconstruct the Trajectory (MFRT) is found by limiting the error between the original and the filtered signals, to 0.05 degrees in angle, and 1 mm in translation over the complete trajectory. This is done by scanning the signals in steps of 3Hz, from 3 to 300Hz and applying filtering. Figure 15 shows pitch moment, and store pitch angle from the trajectory HS2600. The filtering dramatically reduces the spectral content of the moment signal. However, the filtered pitch angle matches perfectly the original signal.

Figure 16 summarises the MFRT frequencies for the different computed cases. The black lines correspond to the frequencies of the cavity modes. As can be seen, different trajectory parameters are driven by different frequency ranges. The longitudinal displacement is dictated by C_x, which is sensitive to frequencies bellow the first cavity mode (24Hz). The span-wise and vertical displacements are dictated by C_y, and C_z respectively, and are driven by frequencies bellow cavity mode 2 (55Hz), with some limited influence of frequencies up to 170Hz in the span-wise direction. The pitch and the yaw angles are on average, influenced by frequencies bellow the third cavity mode(87Hz), and in some cases by frequencies up to 200Hz. Finally, the roll angle is sensitive to frequencies even above 300Hz.

(a) C_x : Longitudinal Force (b) C_y : span-wise Force (c) C_z : Vertical Force

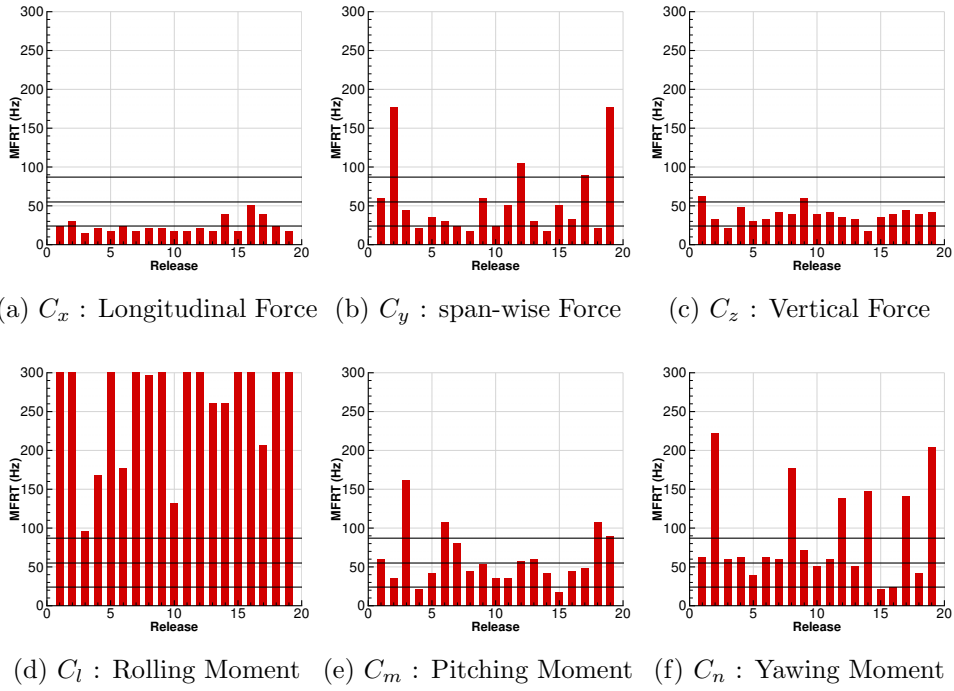(d) C_l : Rolling Moment (e) C_m : Pitching Moment (f) C_n : Yawing Moment

Figure 16: MFRT for the different releases and force/moment coefficients.

Figure 17 shows the filtered loads for the different releases. C_x (Figure 17a) only depends on the store position, meaning that the longitudinal displacement is driven by the mean flow. The filtered C_y, C_l and C_n fluctuate around zero, and are influenced by local asymmetries of flow inside the bay. The filtered C_z and C_m (Figures 17e and 17d) significantly fluctuate around

(a) C_x : Longitudinal Force

(b) C_l : Rolling Moment

(c) C_y : span-wise Force

(d) C_m : Pitching Moment

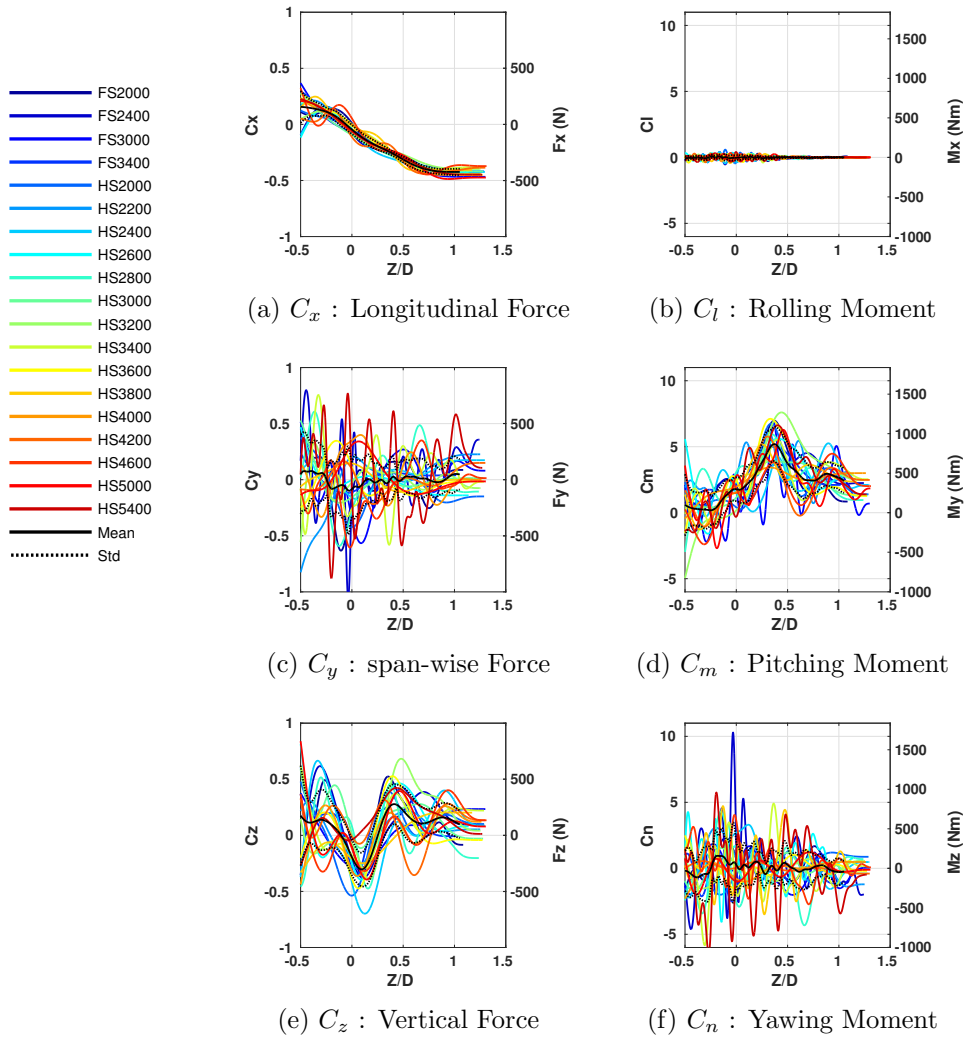(e) C_z : Vertical Force

(f) C_n : Yawing Moment

Figure 17: Filtered force and moment during full and half stroke releases.

the averaged release, and show the largest excursions from it.

The store loads fluctuate under the action of three main pressure contributions. First, the tonal fluctuations caused by standing waves oscillations (typical in cavity flows), lead to variability regarding the time of release [34]. In addition, the turbulence also increases the variability in time, mainly for the roll angle. Finally, the store/shear layer interaction differs depending on the store trajectory history and the instantaneous flowfield. This interaction, and the associated trajectory variability, can be captured only if the loads are fully coupled with the flowfield, which means that coupled CFD/6DoF calculations are needed.

6   Conclusions

Scale-Adaptive Simulations of store release from weapon bays show that it is possible to numerically estimate store trajectory variability. A statistical metric was proposed to identify the minimum number of simulations necessary for capturing the mean and standard deviation of the trajectories. For the store at hand, twelve trajectories were necessary mainly due to variability in roll associated with the low roll inertia. Using the averaged flow data, the trajectory phases were identified and the role of the pressure field inside the cavity was clarified. Then, filtering of the simulation results, revealed that only the roll angle was driven by the finest fluctuations in the flowfield while the vertical displacement of the store was driven by the ejection velocity and gravity. This is reinforced by the relatively low pitch angle of the store during the release, leading to a reduced effect of the aerodynamic lift generated. The present results suggest that the proposed method is efficient and can be used for initial investigations of store clearance before flight testing.

References

[1] Rossiter, J. E., "Wind Tunnel Experiments on the Flow Over Rectangular Cavities at Subsonic and Transonic Speeds," Technical Report 64037, Royal Aircraft Establishment, Bedford, UK, October 1964.

[2] Schmit, R., Grove, J., Semmelmayer, F., and Haverkamp, M., "Nonlinear feedback mechanisms inside a rectangular cavity," *AIAA Journal*, Vol. 52, No. 10, 2014, pp. 2127 – 2142, doi:10.2514/1.J052804.

[3] Loupy, G. and Barakos, G., "Modelling of Transonic Shallow Cavity Flows and Store Release Simulations from Weapon Bays," *Proceedings of the 35th AIAA Applied Aerodynamics Conference*, Paper No. AIAA 2017-3252, American Institute of Aeronautics and Astronautics Inc, Denver, Colorado, United states, 2017, doi:10.2514/6.2017-3252.

[4] Lawson, S. and Barakos, G., "Review of Numerical Simulations For High-Speed, Turbulent Cavity Flows," *Progress in Aerospace Sciences*, Vol. 47, No. 3, 2011, pp. 186 – 216, doi:10.1016/j.paerosci.2010.11.002.

[5] Atkins, D., "Flight Test Results of a GBU-38 Separating from the B-1B Aircraft," *Proceedings of the 46th AIAA Aerospace Sciences Meeting and Exhibit*, Paper No. AIAA 2008-184, American Institute of Aeronautics

and Astronautics Inc, Reno, Nevada, United States, 7-10 January 2008, doi:10.2514/6.2008-184.

[6] Johnson, R., Davis, M., and Finley, D., "Relaxed Fidelity CFD Methods Applied to Store Separation Problems," RTO AVT Symposium on Functional and Mechanical Integration of Weapons and Land and Air Vehicles, Published in RTO-MP-AVT-108, Williamsburg, VA, USA, 7–9 June 2004.

[7] Nayyar, P., Barakos, G. N., and Badcock, K. J., "Numerical study of transonic cavity flows using large-eddy and detached-eddy simulation," *Aeronautical Journal*, Vol. 111, No. 1117, 2007, pp. 153–164, doi:10.1017/S0001924000004413.

[8] Babu, S., Zografakis, G., Barakos, G. N., and Kusyumov, A., "Evaluation of scale-adaptive simulation for transonic cavity flows." *International Journal of Engineering Systems Modelling and Simulation*, Vol. 8, No. 2, 2016, pp. 106–124, doi:10.1504/IJESMS.2016.075510.

[9] Menter, F. and Egorov, Y., "The Scale-Adaptive Simulation Method for Unsteady Turbulent Flow Predictions. Part 1: Theory and Model Description," *Flow, Turbulence and Combustion*, Vol. 85, No. 1, 2010, pp. 113–138, doi:10.1007/s10494-010-9264-5.

[10] Johnson, R. and Cary, A., "F-111 Store Trajectory Analysis," RTO AVT Symposium on Functional and Mechanical Integration of Weapons and Land and Air Vehicles, Published in RTO-MP-AVT-108, Williamsburg, VA, USA, 7–9 June 2004.

[11] Sickles, W., Hand, T., Morgret, C., Masters, J., and Denny, A., "High-fidelity, time-accurate CFD store separation simulations from a B-1B

bay with comparisons to quasi-steady engineering methods," *Proceedings of the 46th AIAA Aerospace Sciences Meeting and Exhibit*, Paper No. AIAA 2008-186, Reno, NV, United States, 7-10 January 2008, doi:10.2514/6.2008-186.

[12] Lee, J., Piranian, A., Martel, J., Crowe, D., and Rizk, M., "Store Separations in Jet Flow Environments," *48th AIAA Aerospace Sciences Meeting*, Paper No. AIAA 2010-510, Orlando, Florida, USA, 4-7 January 2010, doi:10.2514/6.2010-510.

[13] Merrick, J. and Reeder, M., "Sphere release from a rectangular cavity at Mach 2.22 freestream conditions," *Journal of Aircraft*, Vol. 53, No. 3, 2016, pp. 822–829, doi:10.2514/1.C033636.

[14] Kim, D., Choi, J., and Kwon, O., "Detached eddy simulation of weapons bay flows and store separation," *Computers and Fluids*, Vol. 121, 2015, pp. 1–10, doi:10.1016/j.compfluid.2015.07.022.

[15] Lawson, S. J., Steijl, R., Woodgate, M., and Barakos, G. N., "High performance computing for challenging problems in computational fluid dynamics," *Progress in Aerospace Sciences*, Vol. 52, No. 1, 2012, pp. 19–29, doi: 10.1016/j.paerosci.2012.03.004.

[16] Jarkowski, M., Woodgate, M., Barakos, G., and Rokicki, J., "Towards Consistent Hybrid Overset Mesh Methods for Rotorcraft CFD," *International Journal for Numerical Methods in Fluids*, Vol. 74, No. 8, 2014, pp. 543–576, doi:10.1002/fld.3861.

[17] Loupy, G. and Barakos, G., "Processing and Analysis Methods for Transonic Cavity Flow," *Physics of Fluids*, Vol. 29, No. 16, 2017, doi:10.1063/1.4995461.

[18] Barakos, G., Lawson, S., Steijl, R., and Nayyar, P., "Numerical Simulations of High–Speed Turbulent Cavity Flows," *Flow, Turbulence and Combustion*, Vol. 83, No. 4, December 2009, pp. 569–585, doi:10.1007/s10494-009-9207-1.

[19] Siouris, G., *Missile Guidance and Control Systems*, Springer-Verlag New York Inc., 1st ed., 2008.

[20] Nightingale, D., Ross, J., and Foster, G., "Cavity Unsteady pressure measurements - Examples from Wind-Tunnel Tests," Tech. Rep. Version 3, Aerodynamics & Aeromechanics Systems Group, QinetiQ, Bedford, UK, November 2005.

[21] Fox, J., "Generic Wing Pylon, and Moving Finned Store. TN. 37389-6001," Arnold Engineering Development Center (AEDC), Arnold AFB, USA, 2000.

[22] Prewitt, N., Belk, D., and Maple, R., "Multiple-Body Trajectory Calculations Using the Beggar Code," *Journal of Aircraft*, Vol. 36, No. 5, 1999, pp. 802–808, doi:10.2514/2.2513.

[23] Demir, H. and Alemdaroglu, N., "Trajectory Calculation of a Store Released from a Fighter Aircraft," *Proceedings of the 43rd AIAA Aerospace Sciences Meeting and Exhibit*, Paper No. AIAA 2005-847, San Diego, California, USA, 24-27 June 2005, doi:10.2514/6.2005-847.

[24] Lijewski, L. and Suhs, N., "Time-Accurate Computational Fluid Dynamics Approach to Transonic Store Separation Trajectory Prediction," *Journal of Aircraft*, Vol. 31, No. 4, 1994, pp. 886–891, doi:10.2514/3.46575.

[25] Davis, M. and Welterlen, T., "Minimized Domain CFD for Store Separation," *Proceedings of the 41st Aerospace Sciences Meeting and Exhibit*, Paper No. AIAA 2003-1245, Reno, Nevada, USA, 6-9 January 2003, doi:10.2514/6.2003-1245.

[26] Yang, H., Kannan, R., and Przekwas, A., "A Nonlinear Reduced Order Method with Overset Adaptive Cartesian/Unstructured Grid for Moving Body Simulation," *Proceedings of the 50st AIAA Aerospace Sciences Meeting*, Paper No. AIAA 2012-0414, Nashville, Tennessee, USA, 6-9 January 2012, doi:10.2514/6.2012-414.

[27] Oktay, E., Merttopcuoglu, O., and Akay, H., "An Approach for Parallel CFD Solutions of Store Separation Problems," *Parallel Computational Fluid Dynamics 2007*, Vol. 67 of *Lecture Notes in Computational Science and Engineering*, Springer Berlin Heidelberg, 2009, pp. 393–400, doi:10.1007/978-3-540-92744-0_49.

[28] Panagiotopoulos, E. and Kyparissis, S., "CFD Transonic Store Separation Trajectory Predictions with Comparison to Wind Tunnel Investigations," *International Journal of Engineering*, Vol. 3, January 2010, pp. 538 – 553.

[29] Snyder, D., Koutsavdis, E., and Anttonen, J., "Transonic Store Separation Using Unstructured CFD with Dynamic Meshing," *Proceedings of the 33rd AIAA Fluid Dynamics Conference and Exhibit*, Paper No. AIAA 2003-3919, Orlando, Florida, USA, 23-26 June 2003, doi:10.2514/6.2003-3919.

[30] Hooker, J. and Gudenkauf, J., "Application of the Unstructured Chimera Method for Rapid Weapons Trajectory Simulations," *Pro-

ceedings of the 45th AIAA Aerospace Sciences Meeting and Exhibit,
Paper No. AIAA 2007-75, Reno, Nevada, USA, 8-11 January 2007,
doi:10.2514/6.2007-75.

[31] Noack, R. and Boger, D., "Improvements to SUGGAR and DiRTlib for
Overset Store Separation Simulations," *Proceedings of the 47th AIAA
Aerospace Sciences Meeting including The New Horizons Forum and
Aerospace Exposition*, Paper No. AIAA 2009-340, Orlando, Florida,
USA, 5-8 January 2009, doi:10.2514/6.2009-340.

[32] Tang, L., Yang, J., and Lee, J., "Hybrid Cartesian Grid/Gridless Algo-
rithm for Store Separation Prediction," *Proceedings of the 48th AIAA
Aerospace Sciences Meeting Including the New Horizons Forum and
Aerospace Exposition*, Paper No. AIAA 2010-508, Orlando, Florida,
USA, 4-7 January 2010, doi:10.2514/6.2010-508.

[33] Laghari, W., Baloch, M., Mengal, M., and Shah, S., "Performance
Analysis of Analog Butterworth Low Pass Filter as Compared to
Chebyshev Type-I Filter, Chebyshev Type-II Filter and Elliptical
Filter," *Circuits and Systems*, Vol. 5, No. 9, 2014, pp. 209–216,
doi:10.4236/cs.2014.59023.

[34] Murray, N., Jansen, B., Gui, L., Seiner, J., and Birkbeck, R., "Measure-
ments of Store Separation Dynamics," *Proceedings of the 47th AIAA
Aerospace Sciences Meeting including the New Horizons Forum and
Aerospace Exposition*, Paper No. AIAA 2009-105, Orlando, Florida,
USA, 5-8 January 2009, doi:10.2514/6.2009-105.